An Active and Robust Catalytic Architecture of NiCo/GaN NWs for Light-Driven Hydrogen Production from Methanol

Jinglin Li[1+], Bowen Sheng[2+], Yiqing Chen[3+], Jiajia Yang[2], Ping Wang[2], Yixin Li[1], Tianqi Yu[1], Hu Pan[1], Jun Song[3]*, Lei Zhu[1], Xinqiang Wang[2,4,5]*, Tao Ma[6], Baowen Zhou[1]*.

1. Key Laboratory for Power Machinery and Engineering of Ministry of Education, Research Center for Renewable Synthetic Fuel, School of Mechanical Engineering, Shanghai Jiao Tong University, 800 Dongchuan Road, Shanghai 200240, China.
2. State Key Laboratory of Artificial Microstructure and Mesoscopic Physics, School of Physics, Nano-Optoelectronics Frontier Center of Ministry of Education (NFC-MOE), Peking University, Beijing 10087, China.
3. Department of Mining and Materials Engineering, McGill University, 3610 University Street, Montreal, QC H3A0C9, Canada.
4. Peking University Yangtze Delta Institute of Optoelectronics, Nantong, Jiangsu 226010, China.
5. Collaborative Innovation Center of Quantum Matter, School of Physics, Peking University, Beijing 100871, China.
6. Michigan Center for Materials Characterization (MC)^2, University of Michigan, Ann Arbor, MI 48109, USA.

* Corresponding authors Email: jun.song2@mcgill.ca; wangshi@pku.edu.cn; zhoubw@sjtu.edu.cn

+ These authors contributed equally to this work.

Abstract: On-site hydrogen production from liquid organic hydrogen carriers *e.g.*, methanol provides an emerging strategy for the safe storage and transportation of hydrogen. Herein, we

This is the author manuscript accepted for publication and has undergone full peer review but has not been through the copyediting, typesetting, pagination and proofreading process, which may lead to differences between this version and the Version of Record. Please cite this article as doi: 10.1002/smll.202309906.

This article is protected by copyright. All rights reserved.

Author Manuscript

report a catalytic architecture consisting of nickel-cobalt nanoclusters dispersed on gallium nitride nanowires supported by silicon for light-driven hydrogen production from methanol. By correlative microscopic and spectroscopic characterizations, as well as density functional theory calculations, it is revealed that NiCo nanoclusters work in synergy with GaN nanowires to enable the achievement of a significantly reduced activation energy of methanol dehydrogenation by switching the potential-limiting step from *CHO → *CO to *CH_3O → *CH_2O. In combination with the marked photothermal effect, a high hydrogen rate of 5.62 mol·g_{cat}^{-1}·h^{-1} with a prominent turnover frequency of 43460 mol H_2 per mol NiCo per hour is achieved under concentrated light of 5 W·cm^{-2} without any other energies input. Remarkably, the synergy between Co and Ni, in combination with the unique surface of GaN, renders the architecture with outstanding resistance to sintering and coking. The architecture thereby exhibits a high turnover number of >16,310,000 mol hydrogen per mol NiCo over an ultra-long operation testing of 600 h. Outdoor testing validates the viability of the architecture for active and robust hydrogen evolution under natural concentrated sunlight. Overall, this work presents a promising architecture for on-site hydrogen production from liquid organic hydrogen carriers *e.g.*, CH_3OH by virtually unlimited solar energy.

1. Introduction

Hydrogen (H_2) has emerged as an ideal energy carrier for a carbon-neutral economy because of its features of high gravimetric energy (143 MJ/kg) and clean combustion to water.[1-3] Unfortunately, the physical and chemical properties of hydrogen make its storage and transportation substantially challenging.[4] Over the past years, the concept of storing H_2 in liquid organic hydrogen carriers (LOHCs), and on-site hydrogen release from LOHCs in the presence of catalysts has appeared as a promising strategy for addressing the storage and transportation issues of H_2. Owing to the merits of high H_2 content (12.5wt.%), high safety, and high compatibility with the existing infrastructures, methanol is considered an ideal candidate for LOHCs.[5-6] In 2003, the pioneering work for extracting H_2 from methanol (CH_3OH) was conducted over a platinum/aluminum oxide catalyst, opening up a pathway to utilizing CH_3OH for on-site hydrogen production.[7] Since then, considerable efforts have been devoted to releasing hydrogen from CH_3OH by various approaches, mainly focusing on thermo-catalysis (**Fig. S1**).[2, 8] For example, as a landmark breakthrough, a single nuclear Ru-based complex was explored for thermo-catalytic hydrogen generation from methanol with an

This article is protected by copyright. All rights reserved.

Author Manuscript

impressive turnover frequency of 4700 mol hydrogen per mol ruthenium per hour with the assistance of potassium hydroxide.[8] More recently, with the use of atomically dispersed Pt supported by α-MoC catalyst, hydrogen could be produced with a high turnover frequency of 18406 mol H_2 per mol of Pt per hour and a turnover number of 132166 mol H_2 per mol Pt under relatively mild conditions (190 °C, 20 bar) by the only input of thermal energy.[2] Despite notable advances, thermo-catalysis has still suffered from intensive thermal energy input, and/or negative environmental impacts of using strong base additives. From the viewpoint of environmental accountability, it is imperative to explore a green means for H_2 generation from methanol. In recent years, there has been growing research interest in light-driven hydrogen evolution from methanol; and a broad range of photocatalysts *e.g.*, Pt/TiO_2,[9] Pt/CN,[10] and plasmonic ZnCu alloy[4] were developed for this grand topic. Nevertheless, the activity of even state-of-the-art photocatalytic systems is far below practical demands (**Table S1**). Meanwhile, most of the photocatalysts are vulnerable to activity degradation within several hours, remaining a substantial bottleneck of light-driven methanol dehydrogenation.[4, 10-11]

In this study, we focus on assembling a rational catalytic architecture to break the bottleneck of releasing hydrogen from methanol driven by sunlight. Based on our previous discoveries, owing to the excellent optoelectronic properties, GaN nanowires (NWs) vertically aligned on silicon wafer can offer a promising platform for solar-to-fuel conversion *e.g.*, water splitting[12-16] and CO_2 reduction.[17] Of note, GaN NWs with high surface area and unique surface properties are promising for manipulating the catalytic behavior and for endowing the architecture with remarkable sintering- and coking-resistant capability. Such an emerging platform thus exhibits great potential in active and robust hydrogen generation from light-driven methanol dehydrogenation.

Nickel (Ni) has been widely used for catalyzing hydrogen evolution from methanol because of its low cost and suitable catalytic properties.[18-20] However, like many other metals, nanostructured Ni is hampered by fierce metal sintering and coking.[21-22] Recent advances have shown that coupling with a homologous component is viable for improving the activity and durability of nickel by tailoring the geometric and electronic properties,[23] especially when supported by suitable scaffolds. Herein, a novel catalytic architecture is assembled by coupling a binary NiCo cocatalyst onto GaN NWs. The synergy between Ni and Co, coordinating with GaN NWs, endows the architecture with a significantly lowered activation energy as well as

This article is protected by copyright. All rights reserved.

Author Manuscript

Author Manuscript

superior sintering- and coking- resistant capability during the methanol dehydrogenation process. In combination with the marked photo-thermal effect, the architecture demonstrated an impressive hydrogen rate (HR) of 5.62 $mol \cdot g_{cat}^{-1} \cdot h^{-1}$ with a measurable turnover frequency (TOF) of 43460 mol H_2 per mol NiCo per hour under concentrated light of 5 $W \cdot cm^{-2}$. A high turnover number (TON) of 16,310,000 mole H_2 per mole NiCo is thereby achieved over ultra-long durability (DA) testing of >600 h. Experimental and computational investigations suggest that the hybrid of NiCo and GaN NWs switches the potential-limiting step from *CHO→*CO to $*CH_3O \rightarrow *CH_2O$, as well as inhibits the agglomeration of nanoclusters and the formation of coke over the surface, thus leading to a considerable H_2 activity and durability. What is more, outdoor testing confirms the viability of on-site hydrogen evolution from methanol over the as-designed architecture under natural concentrated sunlight with economic and technologic benefits since it can dramatically increase the activity and reduce the usage of the photocatalyst by using a simple and low-cost resin lens for sunlight concentrating. This work presents an active and robust catalytic architecture for hydrogen production from CH_3OH using nearly cost-free concentrated solar energy.

2. Results and discussion

Fabrication and characterization of NiCo/GaN NWs. Based on the reported method,[24] GaN nanowire arrays (NWs) were grown on a 4-inch Si (111) wafer by plasma-assisted molecular beam epitaxy under an N-rich atmosphere (**Experimental section** and **Fig. S2**). The hybridization of GaN NWs and NiCo nanoclusters was conducted by a straightforward photo-deposition method with varied Ni/Co ratios. For comparison, Ni/GaN NWs and Co/GaN NWs were prepared by the identical procedure, and the major difference is the precursors utilized for photo-deposition. As characterized by scanning electron microscopy (SEM), the epitaxial GaN NWs vertically aligned on Si wafer feature an average length of ~900 nm with a diameter of ~60 nm (**Fig. 1A**). The well-defined 1D morphology endows GaN NWs with high specific surface area, which is highly conducive to strengthening photon absorption, shortening the diffusion path of charge carriers, and immobilizing catalytic sites.[25-26] Compared with pristine GaN NWs (**Fig. S3**), the overall morphology of GaN NWs is not varied with the decoration of NiCo nanoclusters. High-angle annular dark-field scanning transmission electron microscopy (HAADF-STEM) characterization demonstrates that NiCo nanoclusters are randomly

This article is protected by copyright. All rights reserved.

distributed on the surface of GaN NWs with an average diameter of ~20 nm (**Fig. 1B**). The lattice spacing of 0.26 nm is attributed to the (002) plane of GaN, suggesting that the growth direction of nanowires is the c-axis. It is well matched with the typical peaks at 2θ of 34.2 degrees by X-ray diffraction (XRD) characterizations (**Fig. S4**). The lattice spacing of 0.20 nm is assigned to the (111) plane of NiCo nanoclusters.[27-28] However, no diffraction peaks belonging to NiCo nanoclusters were detected in XRD patterns, probably owing to its high dispersion and low content (0.044 μmol·cm^{-2} determined by inductively coupled plasma-atomic emission spectroscopy (ICP-OES), in which the Ni and Co is 0.212 and 0.228 μmol·cm^{-2}, respectively (**Table S2**)). The energy-dispersive X-ray spectroscopy (EDS) mapping further confirmed the NiCo nanoclusters were successfully anchored onto the GaN scaffold (**Fig. 1B**).

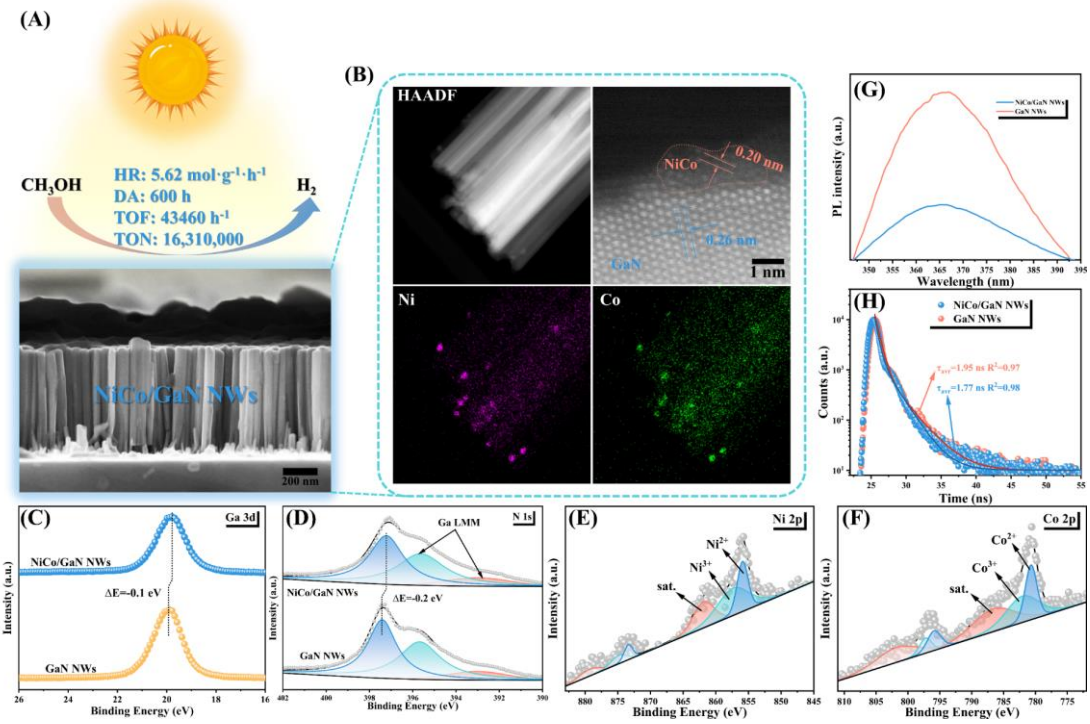


Fig. 1. Structural, chemical, and physical properties of GaN NWs decorated with/without NiCo nanoclusters. (A) Schematic illustration of NiCo/GaN NWs for light-driven hydrogen production from methanol with a 45º-tilted SEM image. (B) HAADF-STEM and EDS mapping images of NiCo-decorated GaN NWs. High-resolution XPS spectra of (C) Ga 3d, (D) N 1s, (E) Ni 2p, and (F) Co 2p. (G) Photoluminescence (PL) spectra of GaN NWs and NiCo/GaN NWs recorded with pulse excitation of 80 MHz at a wavelength of 325 nm. (H) Time-resolved PL (TR-PL) of GaN NWs and NiCo/GaN NWs recorded by a time-correlated single photon counting technique with pulse excitation of 80 MHz at a wavelength of 325 nm.

This article is protected by copyright. All rights reserved.

Author Manuscript

The surface chemical compositions of the as-prepared architectures were studied by X-ray photoelectron spectroscopy (XPS) (**Fig. S5**). The characteristic peaks of Ga 3d and N 1s were detected at ~20 and ~397 eV, respectively (**Figs. 1C** and **1D**).[29] The HR-XPS spectra of Ni 2p and Co 2p in **Figs. 1E** and **1F** show the characteristic peaks of multiple valence states,[30-31] suggesting that NiCo nanocluster is presumably a composite of binary polyvalent metal. Notably, the binding energies of both Ga 3d and N 1s in NiCo/GaN NWs exhibited an obvious shift compared to that of pristine GaN, implying the strong electronic interaction between GaN and NiCo.[29, 32] It is favorable for photoinduced charge carriers transfer and for stabilizing NiCo nanocluster against agglomeration. Moreover, according to the results of UV-vis absorption spectra (**Fig. S6**), the light absorption capability of the semiconductor platform can be enhanced by the introduction of GaN NWs through alleviating photon scattering because of the well-defined nanowire arrays morphology, which is well consistent with our previous study.[33-34] Photoluminescence (PL) spectroscopy characterization shows that the typical peak intensity of GaN is considerably lowered by decorating with NiCo nanoclusters (**Fig. 1G**), indicating inhibited recombination of charge carriers.[35] Time-resolved PL spectra (TRPL) in **Fig. 1H** further validates that the charge carriers' lifetime of GaN NWs is reduced from 1.95 ns to 1.77 ns by decoration with NiCo nanoclusters. These results above suggest efficient separation and transfer of charge carriers due to the decoration of NiCo nanoclusters.[35-36] Together, NiCo/GaN NWs present a promising catalytic architecture for on-site releasing H_2 from methanol with sunlight as the sole energy input, owing to its excellent geometric, optoelectronic, and catalytic properties, which will be elaborately discussed below.

Evaluating hydrogen evolution from methanol in the lab and outdoors. The performance of H_2 evolution from methanol was evaluated in a closed quartz chamber under atmospheric argon. In the lab, a 300 W Xenon lamp equipped with a quartz lens was used as the light source. The influence of the synergy between Ni and Co on the reaction was first studied, and the results are shown in **Fig. 2A**. It is found that owing to the superior optoelectronic properties of GaN NWs/Si, the cocatalysts of either Ni or Co show considerable hydrogen evolution rates, reaching 0.53 and 0.49 $mol \cdot g_{cat}^{-1} \cdot h^{-1}$, respectively. Impressively, supported by the same platform, NiCo nanoclusters illustrate a significantly enhanced H_2 activity of 1.36 $mol \cdot g_{cat}^{-1} \cdot h^{-1}$ at the optimized Ni/Co ratio of 1/1 compared to that of either Ni or Co individually. This

This article is protected by copyright. All rights reserved.

Author Manuscript

result clearly validates the synergy between Ni and Co in promoting hydrogen evolution from methanol. Meanwhile, the loaded amount of NiCo on GaN NWs/Si affected the activity remarkably (**Fig. S7**). The activity increased with the loading content of NiCo, and reached a maximum value of 1.95 mol·g_{cat}^{-1}·h^{-1} at an optimal NiCo content of 0.044 μmol·cm^{-2}. However, with further overloading of NiCo, the activity dramatically decreased to 1.36 mol·g_{cat}^{-1}·h^{-1}. As measured by TEM (**Fig. S8**), the higher loading of NiCo did not lead to a significant increase in the size of the nanoclusters compared with the optimal loading. As suggested by a previous study,[37] the light-shielding effect resulting from the crowded coverage of NiCo can weaken the light absorption capability of GaN NWs, which may be the primary reason for the decreased activity. During methanol dehydrogenation, as measured by gas chromatography (GC), CO was produced with H_2/CO ratios that are much higher than the stoichiometric value of 2 ($CH_3OH \rightarrow 2H_2 + CO$), in concurrent formation of small amounts of CH_4, which was also observed by other groups.[4, 18] As illustrated in **Fig. S7**, the ratio of H_2/CO was varied from 25.1 to 60.0, suggesting the high selectivity of H_2. It is also indicative of the incomplete dehydrogenation of methanol during the process. Furthermore, as measured by gas chromatography-mass spectrometry (GC-MS) and nuclear magnetic resonance (NMR), there was no evident liquid product e.g., CH_2O and HCOOH formation. Herein, the remarkable H_2/CO ratio is primarily due to the inevitable coke deposition during the reaction, as verified by thermogravimetric analysis (TGA) and XPS below. What's more, in the absence of either GaN NWs or NiCo, the architectures of NiCo/Si and GaN NWs are hardly active for hydrogen evolution from methanol under identical conditions (**Figs. S9-S10**). It is thus rationalized that both GaN NWs and NiCo play vital roles in the reaction. GaN NWs enabled the reaction by offering energetic charge carriers, in line with previous studies.[17, 38]

The light intensity-dependent activity of NiCo/GaN NWs was further examined (**Fig. 2B**). It is found that the hydrogen evolution rate over NiCo/GaN NWs shows an obviously increasing trend with the incident light intensity. Under concentrated light illumination of 5 W·cm^{-2}, an impressive rate of 5.62 mol·g_{cat}^{-1}·h^{-1} with a marked turnover frequency (TOF) of 43460 mol H_2 per mol NiCo nanoclusters per hour was achieved. It is nearly 1-3 orders of magnitude higher than that of state-of-the-art photocatalytic systems under comparable conditions (**Table S1**).[2, 4] Of note, under concentrated light illumination, the photothermal effect on the reaction was inevitable. As measured by an infrared thermal imager, as the light

This article is protected by copyright. All rights reserved.

Author Manuscript

intensity increased from 3W·cm^{-2} to 5 W·cm^{-2}, the surface temperature of the sample raised up to 409 ℃ from 272 ℃ (**Figs. S11-S12**), which is sufficient for methanol dehydrogenation. Meanwhile, the light-driven hydrogen rate far outstrips the pure thermo-catalytic activity under the same temperatures (**Fig. 2B**). Specifically, the H_2 activity of 1.95 mol·g_{cat}^{-1}·h^{-1} obtained under 3W·cm^{-2} is nearly 23.9 times higher than that of the pure thermo-catalytic activity under the same temperature. Hence, methanol dehydrogenation that occurred under concentrated light did not primarily proceed via thermo-catalysis caused by concentrated light. As calculated by the Arrhenius equation, in the presence of light illumination, the apparent activation energy of methanol dehydrogenation markedly dropped from 3.69 eV to 2.86 eV (**Fig. 2C**), suggesting that the photoinduced charge carriers can efficiently facilitate the activation of reactant molecules.[4, 39] To further investigate the heat-charge effect, the apparent quantum efficiency (AQE) of NiCo/GaN NWs under different monochromatic light irradiation, a critical descriptor of photocatalysis, was calculated. As shown in **Fig. S13**, the AQE of NiCo/GaN NWs at the wavelength of 275 nm under 220 ℃ is as high as 13%. As expected, the corresponding AQE values at 420 nm, 535 nm, and 730 nm monochromatic light illumination showed a substantial drop without varying any other experimental conditions, which is similar to the pure thermocatalytic activity. It can be attributed to that the photons of >365 nm can't produce excited charge carriers since their energy is lower than the bandgap of GaN (3.4 eV). According to the above results, it is reasonable to speculate that the synergy between photo- and thermal-effects plays a crucial role in the measurable activity of methanol dehydrogenation toward H_2. The concentrated light contributed to the outstanding activity via a thermal-assisted photocatalysis process. For NiCo/GaN NWs, in the catalytic cycle, high-energy photons of <365 nm enabled the generation of photoexcited charge carriers (**Fig. 1G**). In combination with the remarkable photothermal effect of visible light and infrared light, the architecture thus demonstrated a measurable activity of hydrogen generation from methanol. Together, such a thermal-assisted photocatalysis shows a promising means for maximizing the utilization of solar energy to release hydrogen from methanol by effectively utilizing different photons at various regions over such a rational catalytic architecture of NiCo/GaN NWs supported by silicon substrate. The durability of the architectures, a key metric for practical application, was also tested. Thrillingly, a high turnover number (TON) of 16,310,000 moles of hydrogen per mole of NiCo was achieved over NiCo/GaN NWs over a long-term testing of >600 hours (**Fig.**

This article is protected by copyright. All rights reserved.

Author Manuscript

2D). As a contrast, either Ni- or Co-decorated GaN NWs exhibits dramatic activity degradation during a short-term operation of 30 hours, giving rise to an inappreciable TON. These results validate the superior activity and durability of NiCo/GaN NWs for light-driven hydrogen production from methanol without any other energies. However, after stability test, this architecture exhibited an obvious activity degradation. As characterized by the SEM and XPS, it may be due to the deformation of GaN NWs from the silicon substrate (**Fig. S14A**), as well as the etching of NiCo nanoparticles from GaN NWs/Si during methanol dehydrogenation (**Figs. S14B** and **C**).

To test the practical viability of the assembled architecture for light-driven hydrogen production from methanol, outdoor experiments were conducted under natural concentrated sunlight at a variable intensity range of 1 to 9 $W \cdot cm^{-2}$, which was varied with the real-time weather (**Fig. 2E**). It is of worthy noting that natural sunlight was concentrated by a very simple and cheap resin lens, which is of considerable benefits to improve the activity and reduce the usage of high-cost photocatalysts, thus technologically and economically benefiting methanol dehydrogenation. The tests were conducted from 10:00 to 14:00 on a sunny day, with the performances being documented every hour. As shown in **Fig. 2F**, at the beginning of 10:00-11:00, only a slight activity of 0.02 $mol \cdot g_{cat}^{-1} \cdot h^{-1}$ was recorded, which was primarily due to the mild light intensity (around 1 $W \cdot cm^{-2}$). As time went on, the activity of hydrogen evolution was considerably improved, and a superior activity of 4.52 $mol \cdot g_{cat}^{-1} \cdot h^{-1}$ was obtained at 13:00-14:00 (**Fig. S15**). The improved activity originates from the increasing sunlight intensity, which can be well explained by the light intensity-dependent activity test in the lab (**Fig. 2B**). After a total 8 hours of operation, a remarkable TON of 121700 moles of H_2 per mole of NiCo was obtained under natural concentrated sunlight condition (**Fig. S16**). The outdoor test validates the superior viability of using this architecture for on-site hydrogen production from liquid organic hydrogen carriers like methanol with the only input of natural sunlight.

Author Manuscript

This article is protected by copyright. All rights reserved.

Author Manuscript

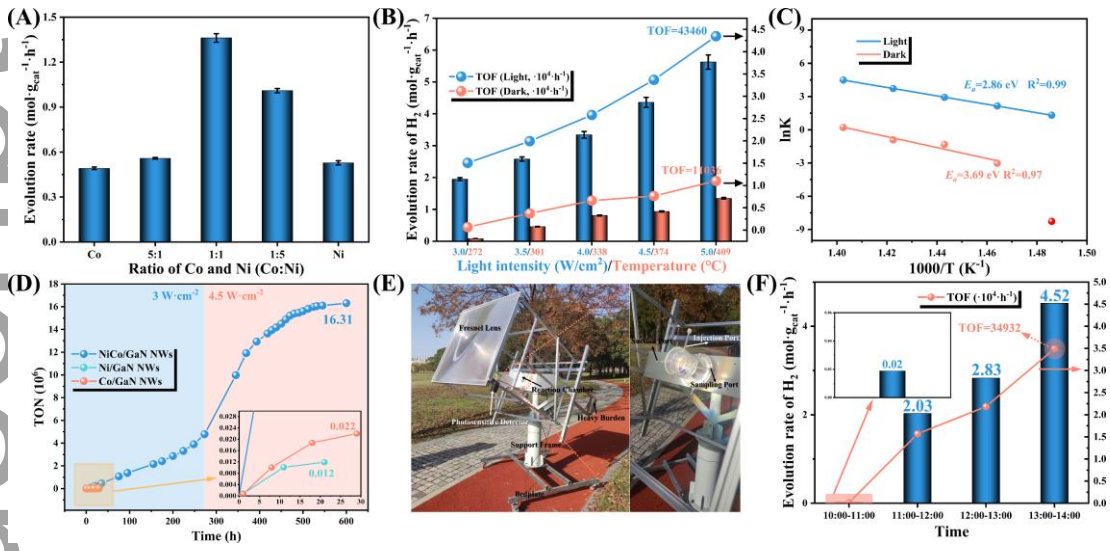


Fig. 2. On-site H_2 evolution from liquid organic hydrogen carrier of methanol. (A) Influence of the synergy between Ni and Co on the activity. The error bars are 0.49 ± 1.7%standard error of mean (s.e.m.) for pure Co, 0.56 ± 0.95%s.e.m. for the ratio of 5:1, 1.36 ± 2.1%s.e.m. for the ratio of 1:1, 1.01 ± 1.4%s.e.m. for the ratio of 1:5, and 0.53 ± 2.6%s.e.m. for pure Ni. (B) H_2 evolution rate and TOF over NiCo/GaN NWs under concentrated light illumination with different intensities and under dark with related temperatures. The error bars are 1.95 ± 2.3%s.e.m. for 3.0 W·cm^{-2}, 2.58 ± 2.6%s.e.m. for 3.5 W·cm^{-2}, 3.34 ± 3.1%s.e.m. for 4.0 W·cm^{-2}, 4.36 ± 3.6%s.e.m. for 4.5 W·cm^{-2}, and 5.62 ± 4.0 %s.e.m. for 5.0 W·cm^{-2}. The error bars are 0.082 ± 0.76%s.e.m. for 272 °C, 0.46 ± 1.1%s.e.m. for 301 °C, 0.81 ± 1.7%s.e.m. for 338 °C, 0.93 ± 2.1%s.e.m. for 374 °C, and 1.3 ± 1.9%s.e.m. for 409 °C. (C) Arrhenius plots for H_2 production rate under the dark and under light-illuminating conditions over NiCo/GaN NWs. (D) Durability test over GaN NWs decorated with various cocatalysts. Experimental conditions for (A), (B), and (D): photocatalyst, ~0.5 cm^2, ~0.34 mg·cm^{-2}; atmospheric argon; 300 W Xenon lamp. (E) Image of outdoor test device equipped with NiCo/GaN NWs at Shanghai Jiao Tong University, Shanghai, P. R. China. (F) Activity and TOF of NiCo/GaN NWs recorded at different times under natural sunlight conditions: 1 W·cm^{-2}~9 W·cm^{-2}. 15-Dec-2022: ambient temperature: 9~11 °C; air humidity: 41%~53%. 17-Dec-2022: ambient temperature: 3~4 °C; air humidity: 40%~48%.

Reaction mechanism. To investigate the reaction mechanism of methanol dehydrogenation at the molecular level, *operando* diffuse reflectance infrared Fourier-transform (DRIFT)

This article is protected by copyright. All rights reserved.

spectroscopy and *in situ* electron paramagnetic electron spectroscopy (EPR) characterization were correlatively conducted to study the evolution track of CH_3OH-to-H_2 conversion. As shown in **Fig. 3A**, the typical peaks at around 1050 and 2950 cm^{-1} are assigned to the adsorbed $*CH_3O$ species,[4, 40-41] which primarily originates from the O-H bond cleavage of CH_3OH. It is well matched with the *in situ* EPR results in **Fig. 3B**, showing the appearance of the OCH_3 radicals. Moreover, the intensities of the two peaks at around 1713 and 1420 cm^{-1} arising from the vibration bands of υ(CO) and δ(CH) in the $*CH_2O$ intermediate increases considerably with the illumination time.[40, 42] This observation reveals the successive dehydrogenation of $*CH_3O$ species toward $*CH_2O$. Furthermore, owing to the eventual deprotonation of the intermediate, *CO is observed at around 2071 cm^{-1},[43] which can be released from the catalytic interface as detected by GC. Together with the GC-MS and NMR characterizations as discussed above, the *operando* DRIFT and *in situ* EPR characterizations present a clear chemical process of CH_3OH dehydrogenation toward H_2 over NiCo/GaN NWs/Si without obvious formation of liquid-phase products such as CH_2O and HCOOH.

DFT calculations were further performed to investigate the reaction pathway. Three surface models, namely GaN ($10\bar{1}0$), Ni/GaN, and NiCo/GaN were first constructed (**Fig. S17**). It is observed that for all three surface models, the exposed GaN surface is the preferred adsorption site for methanol (**Fig. 3C** and **Figs. S18-S19**). Specifically, upon adsorption, the methanol molecule strongly interacts with GaN surface, with the O atom binding to the Ga atom. The N atom nearby strongly attracts the H atom in hydroxyl and splits the methanol molecule, resulting in the effortless formation of $*CH_3O$ intermediate. This finding indicates that GaN NWs is suitable for adsorbing and activating methanol molecules owing to its unique surface properties. Moreover, the free energy diagram demonstrates that the process of $CH_3OH \rightarrow *CH_3O + *H$ on three substrates is highly exergonic, which is also indicative of the strong interplay between the reactant and the catalytic interface. Although GaN ($10\bar{1}0$) can strongly adsorb CH_3OH, it shows a remarkable energy barrier of 1.35 eV through a potential-limiting step of *CO formation (**Fig. 3C**). The decoration of Ni nanocluster on the GaN surface slightly decreases the energy barrier of *CO formation to 1.25 eV, indicating the promotion effect of individual metal on the reaction to some extent. It is very interesting that coupling Co with Ni onto the GaN surface can significantly promote *CO formation by weakening the *CHO binding and switch the potential-limiting step from $*CHO \rightarrow *CO$ to $*CH_3O \rightarrow *CH_2O$,

This article is protected by copyright. All rights reserved.

Author Manuscript

with a much lower ΔG of 0.75 eV. This theoretical discovery presents solid support that Ni works in synergy with Co to significantly reduce the reaction energy barrier for methanol dehydrogenation toward H_2 in the presence of GaN, thus contributing to the considerable activity.

On the basis of the above results, a possible reaction mechanism was proposed for light-driven methanol dehydrogenation over NiCo/GaN NWs/Si (**Fig. 3D**). Under concentrated light illumination, the charge carriers inside GaN are photoexcited by UV light and subsequently migrate to the architecture surface, then jointly drive methanol dehydrogenation with the assistance of the thermo effect caused by visible and near-infrared light. The presence of NiCo nanoparticles improved the migration of photoinduced charge carriers and reduced the recombination rate, thus facilitating the redox reaction over the surface. In the catalytic process, the adsorbed CH_3OH molecules were oxidized in the evolution order of $*CH_3OH \rightarrow *CH_3O \rightarrow *CH_2O \rightarrow *CO$ with the participation of photoinduced holes, and the H^+ released from intermediates were reduced towards H_2 with the assistance of photoinduced electrons. During the continuous dehydrogenation process, NiCo works synergetic with GaN facilitating *CO formation by weakening the CHO binding, and switching the potential-limiting step to $*CH_3O \rightarrow *CH_2O$, thus significantly reducing the energy barrier of methanol dehydrogenation. Consequently, the outstanding synergistic effect between GaN and NiCo, in cooperation with the photo-thermal effect, endows the NiCo/GaN NWs with an excellent capacity for activating methanol molecules, thus enabling a considerable photocatalytic H_2 production from methanol.

Author Manuscript

This article is protected by copyright. All rights reserved.

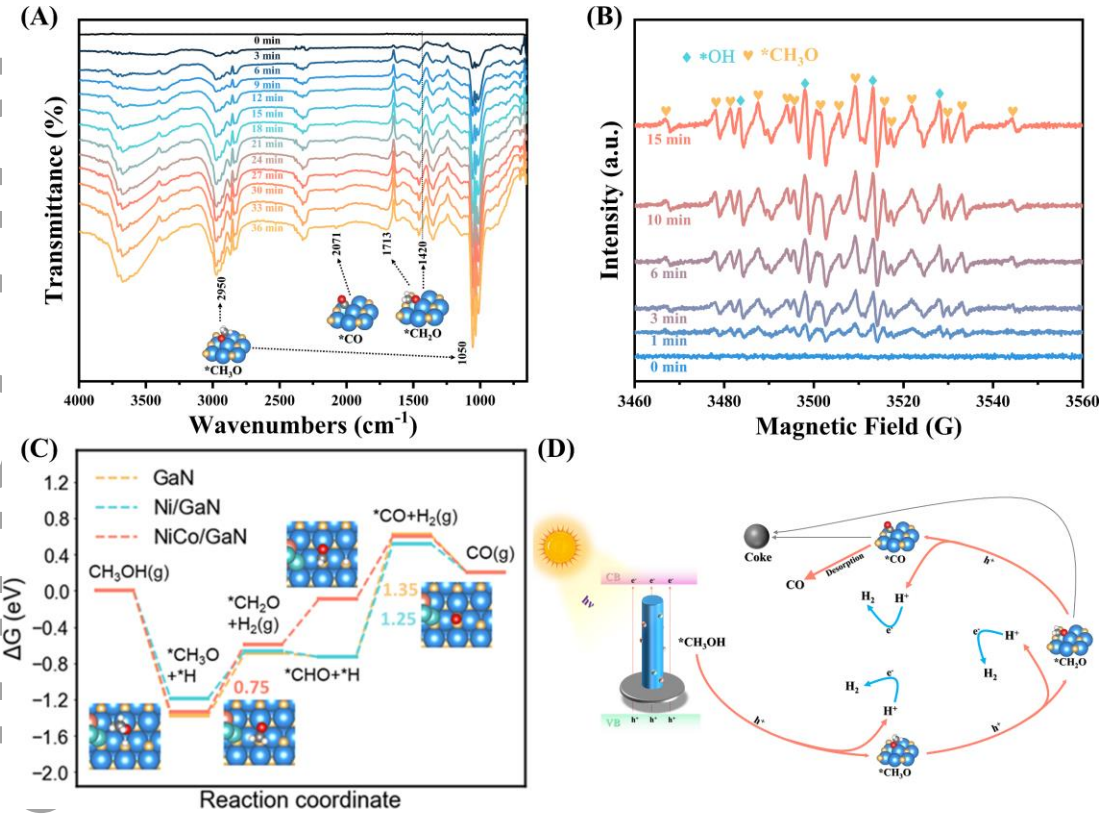


Fig. 3. (A) *Operando* DRIFT spectra of hydrogen production from methanol over NiCo/GaN NWs under the light intensity of 3 W·cm^{-2}. (B) *In situ* EPR spectra of hydrogen production from methanol over NiCo/GaN NWs under a light intensity of 3 W·cm^{-2}. (C) The calculated free energy (ΔG) diagrams for methanol reforming reaction on the three substrates of GaN ($10\bar{1}0$), Ni/GaN, and NiCo/GaN, respectively. The values (in the unit of eV) in the figures indicate the energy barriers for the potential-limiting step of the reaction on the three substrates. Ga, blue; N, yellow; Ni, cyan; Co, orange; C, grey; O, red; and H, white. (D) A proposed mechanism of photocatalytic hydrogen production from methanol over NiCo/GaN NWs. h^+, hole; e^-, electron; h, Planck's constant; ν, frequency.

Origin of the outstanding durability. Durability is one critical metric of the architecture for practical applications. Metal sintering and coking have been widely recognized as the two major causes of catalytic activity degradation during methanol dehydrogenation.[21] To shed light on the prominent durability, metal sintering of the architecture was first studied. To simulate the sintering effect, the architectures were calcinated for varied hours under enhanced conditions at a high temperature of 480 °C, which is higher than the experimental condition. The morphological variation was then characterized by TEM. As described in **Fig. 4A**, in the

This article is protected by copyright. All rights reserved.

Author Manuscript

architecture, the platform of GaN NWs/Si did not show notable change after calcination owing to its outstanding thermal stability.[44] However, the size of anchored Ni nanoclusters obviously grew from ~5.3 nm to ~41.5 nm with an increasing factor of about 7.8 after calcination for 120 h under 480 °C, suggesting the fierce sintering of single Ni (**Fig. S20**). In sharp contrast, the agglomeration rate of NiCo nanoclusters was much slower than that of individual Ni with an increasing factor of 1.7 under identical conditions (**Fig. 4B**). Hence, it is rationalized that the incorporation of Co can significantly improve the sintering-resistant capability of Ni.

Coking, as another key reason for deactivation, was correlatively studied by TGA, XPS, as well as DFT calculations, and the results are shown in **Figs. 4C**, **4D**, and **4E**, respectively. As measured by TGA, within the first 25 h of the reaction, the coking content on NiCo/GaN NWs only reached 0.11%, which was lower than that of Ni/GaN NWs (0.16%) (**Fig. 4C**). The coking content on NiCo/GaN NWs gently increased with the reaction time, and reached 0.23% at 100 h. In stark contrast, the coking content of Ni/GaN NWs approached 0.48% under identical conditions. Compared to Ni/GaN NWs, NiCo/GaN NWs exhibits a much lower coking rate (**Fig. S21**), as confirmed by XPS (**Fig. 4D**). The typical peaks of C 1s of NiCo/GaN NWs are obviously lower than that of Ni/GaN NWs under the same experimental conditions. These results validate the superior coking-resistant capability of NiCo/GaN NWs compared to Ni/GaN NWs. DFT calculations were then conducted to provide a substantial explanation for the lower coking rate of NiCo/GaN NWs. The calculated free energy diagrams for coke formation on three substrates *i.e.*, GaN ($10\bar{1}0$), Ni/GaN and NiCo/GaN, are shown in **Fig. 4D** and with the optimized geometries of the adsorbed intermediates presented in **Figs. 4D** and **S22**. Obviously, owing to the unique surface, GaN ($10\bar{1}0$) is highly coke-resistant with a very high energy barrier of 3.39 eV for forming *C and *O species. However, by adding Ni cluster onto GaN, the energy barrier is significantly reduced to 0.72 eV, as Ni can strongly bind the *O intermediate. It plays an essential descriptor of facile coke formation on Ni/GaN and thus lowers the durability of the architecture. Interestingly, the incorporation of Co atoms to Ni cluster will in turn increase the energy barrier of *C formation to an appropriate value of 1.41 eV, which efficiently improves the coking resistance. These discoveries agree well with the experimental results in **Fig. 2D** and XPS characterizations in **Fig. 4D**. Therefore, the synergy between Ni and Co, in coordination with the unique surface of GaN, bestows remarkable

This article is protected by copyright. All rights reserved.

Author Manuscript

sintering- and coking-resistant capability on the architecture, thus promising to achieve benchmarking durability.

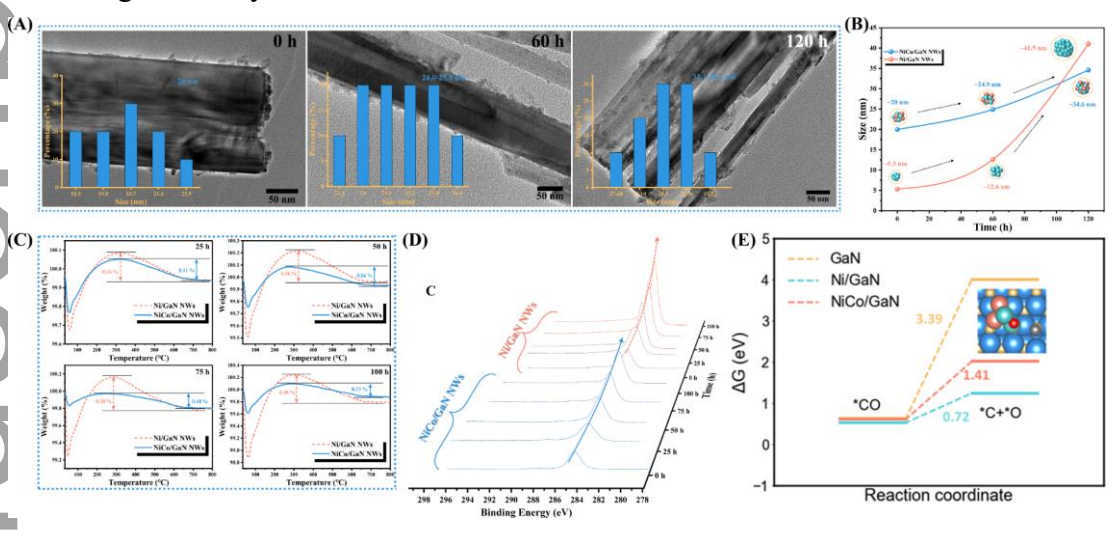


Fig. 4. (A) TEM images and diameters distribution of NiCo/GaN NWs under calcination at 480 ℃ for varied time (0, 60, and 120 h). (B) The calculated size variation of metal nanoclusters under calcination at 480 ℃ for different times. (C) Thermogravimetric plots and (D) HR-XPS spectra of C 1s of NiCo/GaN NWs and Ni/GaN NWs under various illumination reaction time (25, 50, 75, and 100 h). (E) The calculated free energy diagrams for *C species formation on GaN ($10\bar{1}0$), Ni/GaN, and NiCo/GaN.

3. Conclusion

In summary, an active and robust architecture that is primarily composed of NiCo nanoclusters and GaN NWs vertically aligned on silicon wafer has been explored for on-site hydrogen production from light-driven methanol dehydrogenation. Experimental and computational investigations revealed that NiCo worked in synergy with GaN to switch the potential-determining step from *CHO → *CO toward $*CH_3O$ → $*CH_2O$ with a significantly reduced reaction energy barrier. In combination with the remarkable photo-thermal effect, the architecture demonstrated a marked H_2 activity of 5.62 $mol \cdot g_{cat}^{-1} \cdot h^{-1}$ under concentrated light of 5 $W \cdot cm^{-2}$ without any extra energies. In-situ spectroscopic characterizations and DFT calculations showed the chemical process of methanol dehydrogenation toward H_2 without evident formation of liquid product. What is more, the cooperation between Co and Ni, together with the unique surface of GaN, renders the architecture with outstanding resistance to sintering and coking, the architecture thereby exhibited a very high turnover number of >16,310,000 mol hydrogen per mol NiCo over an ultralong operation testing of 600 h. Outdoor testing confirmed

This article is protected by copyright. All rights reserved.

Author Manuscript

the viability of utilizing this architecture for efficient and durable hydrogen evolution from methanol under naturally concentrated sunlight. This work presents an architecture for efficient and durable hydrogen production from methanol, thus practically promising to break the bottleneck of hydrogen storage and transportation using LOHCs and virtually unlimited solar energy.

Data availability

The data supporting the findings of this study are available in the paper and its Supporting Information.

Acknowledgments

The authors are thankful for the financial support from the National Key Research and Development Program of China (2023YFB4004900), Shanghai Pilot Program for Basic Research-Shanghai Jiao Tong University (No. 21TQ1400211), the National Natural Science Foundation of China (No. 22109095), Shanghai Municipal Science and Technology Major Project, and the Oceanic Interdisciplinary Program of Shanghai Jiao Tong University (No. SL2022MS007). B. S., J. Y., and X. W. are thankful for the financial support from the Beijing Outstanding Young Scientist Program (No. BJJWZYJH0120191000103), the Nation Natural Science Foundation of China (No.6230031805), and the Beijing Natural Science Foundation (No. Z200004). J. S. and Y. C. thank the financial support from the Natural Sciences and Engineering Research Council of Canada (NSERC) Discovery grant (No. RGPIN-2017-05187) and computing resources from Digital Research Alliance of Canada.

Author contributions

J. L. and B. Z. conceived the project. J. L. conducted the complete experimental research. B. S., J. Y., and X. W performed to the growth of the supporting material. Y. C. and J. S. contributed to the DFT calculations. Y. L., T. Y., P. W., H. P., and L. Z. conducted the analysis of the experimental data and polished the writing. T. M. performed the STEM and EDS mapping characterization. J. L., Y. C., J. S., and B. Z. wrote the paper with contributions from all co-authors. B. Z. led the research.

Competing interests

This article is protected by copyright. All rights reserved.

Author Manuscript

The authors declare no competing interests.

References

[1] M. Z. Jacobson, W. Colella, D. Golden, *Science* **2005**, 308, 1901.

[2] L. Lin, W. Zhou, R. Gao, S. Yao, X. Zhang, W. Xu, S. Zheng, Z. Jiang, Q. Yu, Y. W. Li, C. Shi, X. D. Wen, D. Ma, *Nature* **2017**, 544, 80.

[3] B. C. Steele, A. Heinzel, in Materials for Sustainable Energy: A Collection of Peer-Reviewed Research and Review Articles from Nature Publishing Group, World Scientific, 2011.

[4] S. Luo, H. Lin, Q. Wang, X. Ren, D. Hernandez-Pinilla, T. Nagao, Y. Xie, G. Yang, S. Li, H. Song, M. Oshikiri, J. Ye, *J. Am. Chem. Soc.* **2021**, 143, 12145.

[5] L. N. Chen, K. P. Hou, Y. S. Liu, Z. Y. Qi, Q. Zheng, Y. H. Lu, J. Y. Chen, J. L. Chen, C. W. Pao, S. B. Wang, Y. B. Li, S. H. Xie, F. D. Liu, D. Prendergast, L. E. Klebanoff, V. Stavila, M. D. Allendorf, J. Guo, L. S. Zheng, J. Su, G. A. Somorjai, *J. Am. Chem. Soc.* **2019**, 141, 17995.

[6] P. Preuster, C. Papp, P. Wasserscheid, *Acc Chem Res* **2017**, 50, 74.

[7] J. Shabaker, R. Davda, G. Huber, R. Cortright, J. Dumesic, *J. Catal.* **2003**, 215, 344.

[8] M. Nielsen, E. Alberico, W. Baumann, H.-J. Drexler, H. Junge, S. Gladiali, M. Beller, *Nature* **2013**, 495, 85.

[9] G. Wu, T. Chen, X. Zong, H. Yan, G. Ma, X. Wang, Q. Xu, D. Wang, Z. Lei, C. Li, *J. Catal.* **2008**, 253, 225.

[10] Y. Wang, E. P. Yao, L. Wu, J. Feldmann, J. K. Stolarczyk, *Angew. Chem. Int. Ed.* **2021**, 60, 26694.

[11] H. Wang, H. Qi, X. Sun, S. Jia, X. Li, T. J. Miao, L. Xiong, S. Wang, X. Zhang, X. Liu, A. Wang, T. Zhang, W. Huang, J. Tang, *Nat. Mater.* **2023**, 22, 619.

[12] P. Zhou, I. A. Navid, Y. Ma, Y. Xiao, P. Wang, Z. Ye, B. Zhou, K. Sun, Z. Mi, *Nature* **2023**, 613, 66.

[13] B. Zhou, X. Kong, S. Vanka, S. Chu, P. Ghamari, Y. Wang, N. Pant, I. Shih, H. Guo, Z. Mi, *Nat. Commun.* **2018**, 9, 1.

[14] D. Wang, A. Pierre, M. G. Kibria, K. Cui, X. Han, K. H. Bevan, H. Guo, S. Paradis, A.-R. Hakima, Z. Mi, *Nano Lett.* **2011**, 11, 2353.

[15] Y. Li, S. M. Sadaf, B. Zhou, *FRONT ENERGY* **2023**.

This article is protected by copyright. All rights reserved.

Author Manuscript

[16] B. Zhou, S. Sun, *FRONT ENERGY* **2023**.
[17] R. T. Rashid, Y. Chen, X. Liu, F. A. Chowdhury, M. Liu, J. Song, Z. Mi, B. Zhou, *Proc. Natl. Acad. Sci. U.S.A.* **2022**, 119, e2121174119.
[18] L. Lin, Q. Yu, M. Peng, A. Li, S. Yao, S. Tian, X. Liu, A. Li, Z. Jiang, R. Gao, X. Han, Y. W. Li, X. D. Wen, W. Zhou, D. Ma, *J. Am. Chem. Soc.* **2021**, 143, 309.
[19] J. Gonzalez-Cobos, V. J. Rico, A. R. Gonzalez-Elipe, J. L. Valverde, A. de Lucas-Consuegra, *ACS Catal.* **2016**, 6, 1942.
[20] G. W. Huber, J. W. Shabaker, J. A. Dumesic, *Science* **2003**, 300, 2075.
[21] B. Gu, M. Bahri, O. Ersen, A. Khodakov, V. V. Ordomsky, *ACS Catal.* **2018**, 9, 991.
[22] M. Akri, S. Zhao, X. Li, K. Zang, A. F. Lee, M. A. Isaacs, W. Xi, Y. Gangarajula, J. Luo, Y. Ren, Y. T. Cui, L. Li, Y. Su, X. Pan, W. Wen, Y. Pan, K. Wilson, L. Li, B. Qiao, H. Ishii, Y. F. Liao, A. Wang, X. Wang, T. Zhang, *Nat Commun.* **2019**, 10, 5181.
[23] J. Wang, Y. Fu, W. Kong, S. Li, C. Yuan, J. Bai, X. Chen, J. Zhang, Y. Sun, *ACS Catal.* **2022**, 12, 4382.
[24] J. Li, B. Sheng, Y. Chen, S. M. Sadaf, J. Yang, P. Wang, H. Pan, T. Ma, L. Zhu, J. Song, H. Lin, X. Wang, Z. Huang, B. Zhou, *Commun. Chem.* **2022**, 5.
[25] J. Deng, Y. Su, D. Liu, P. Yang, B. Liu, C. Liu, *Chem. Rev.* **2019**, 119, 9221.
[26] Y. Su, C. Liu, S. Brittman, J. Tang, A. Fu, N. Kornienko, Q. Kong, P. Yang, *Nat. Nanotechnol.* **2016**, 11, 609.
[27] H. Xu, Z. X. Shi, Y. X. Tong, G. R. Li, *Adv. Mater.* **2018**, 30, e1705442.
[28] Y. Fu, H.-Y. Yu, C. Jiang, T.-H. Zhang, R. Zhan, X. Li, J.-F. Li, J.-H. Tian, R. Yang, *Adv. Funct. Mater.* **2018**, 28.
[29] W. J. Dong, I. A. Navid, Y. Xiao, J. W. Lim, J. L. Lee, Z. Mi, *J. Am. Chem. Soc.* **2021**, 143, 10099.
[30] W. Zhu, W. Chen, H. Yu, Y. Zeng, F. Ming, H. Liang, Z. Wang, *Appl. Catal. B* **2020**, 278.
[31] Y. Xiao, P. Zhang, X. Zhang, X. Dai, Y. Ma, Y. Wang, Y. Jiang, M. Liu, Y. Wang, *J. Mater. Chem. A* **2017**, 5, 15901.
[32] T. Duan, J. Pan, D. S. Ang, *Appl. Phys. Lett.* **2013**, 102, 201604.
[33] B. Zhou, X. Kong, S. Vanka, S. Chu, P. Ghamari, Y. Wang, N. Pant, I. Shih, H. Guo, Z. Mi, *Nat. Commun.* **2018**, 9, 3856.
[34] B. Zhou, J. Li, X. Dong, L. Yao, *Sci China Chem* **2023**, 66, 739.

This article is protected by copyright. All rights reserved.

Author Manuscript

[35] Z. Zhang, Y. Liang, H. Huang, X. Liu, Q. Li, L. Chen, D. Xu, *Angew. Chem. Int. Ed.* **2019**, 58, 7263.

[36] Q. Y. Shen, T. Y. Xu, G. L. Zhuang, Y. Zhuang, L. M. Sun, X. G. Han, X. J. Wang, W. W. Zhan, *ACS Catal.* **2021**, 11, 12931.

[37] J. Low, J. Yu, M. Jaroniec, S. Wageh, A. A. Al-Ghamdi, *Adv. Mater.* **2017**, 29.

[38] M. Kibria, S. Zhao, F. Chowdhury, Q. Wang, H. Nguyen, M. Trudeau, H. Guo, Z. Mi, *Nat. Commun.* **2014**, 5, 3825.

[39] X. Bian, Y. Zhao, G. I. N. Waterhouse, Y. Miao, C. Zhou, L.-Z. Wu, T. Zhang, *Angew. Chem. Int. Ed.* **2023**, e202304452.

[40] V. Lochař, *APPL CATAL A-GEN* **2006**, 309, 33.

[41] B. Frank, F. C. Jentoft, H. Soerijanto, J. Kröhnert, R. Schlögl, R. Schomäcker, *J. Catal.* **2007**, 246, 177.

[42] D. B. Clarke, D.-K. Lee, M. J. Sandoval, A. T. Bell, *J. Catal.* **1994**, 150, 81.

[43] J. Weigel, R. Koeppel, A. Baiker, A. Wokaun, *Langmuir* **1996**, 12, 5319.

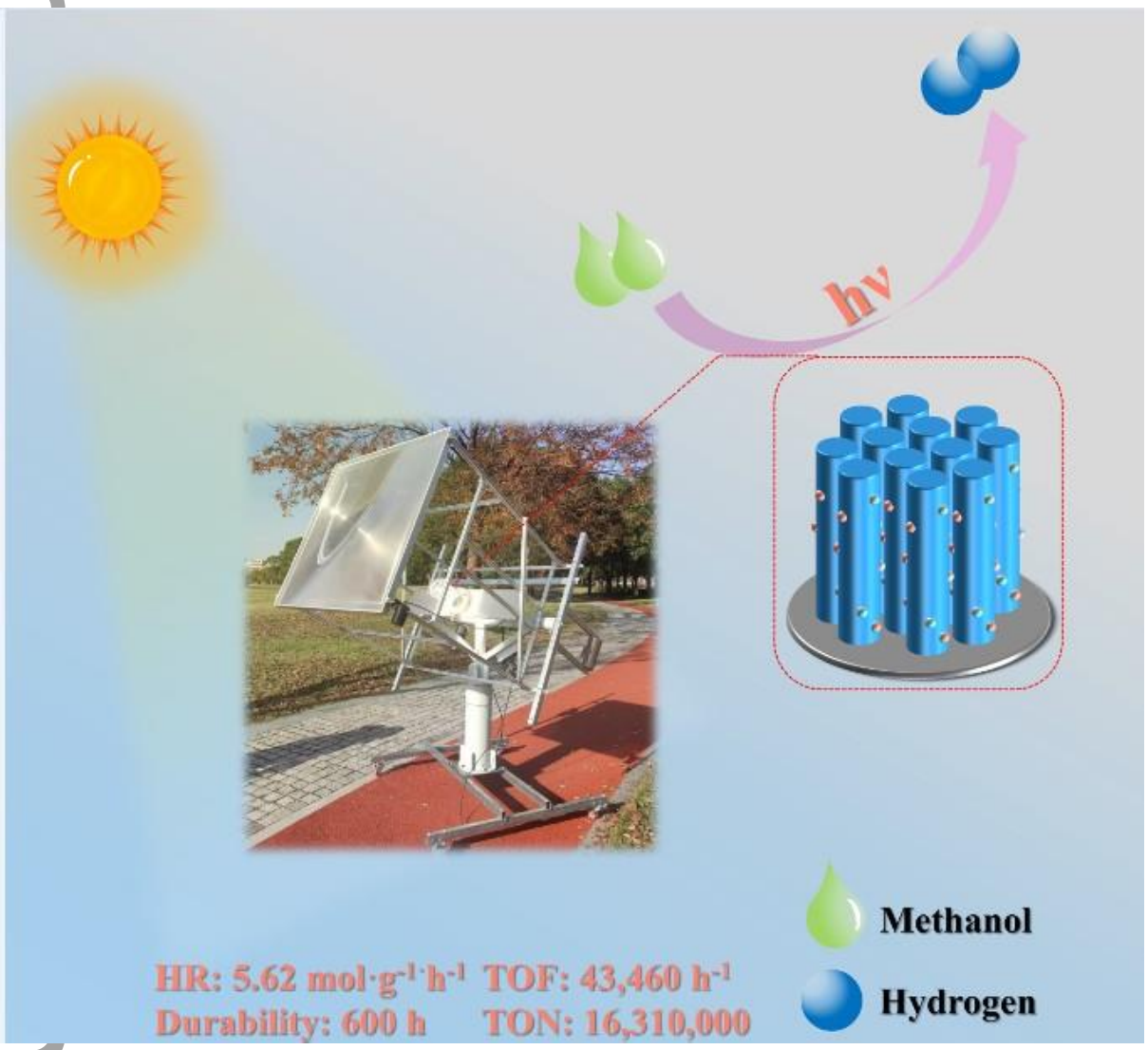
[44] S. Sheng, T. Wang, S. Liu, F. Liu, B. Sheng, Y. Yuan, D. Li, Z. Chen, R. Tao, L. Chen, B. Zhang, J. Yang, P. Wang, D. Wang, X. Sun, J. Zhang, J. Xu, W. Ge, B. Shen, X. Wang, *Adv. Sci.* **2022**, 9, e2106028.

Herein, we assembled a novel architecture by coupling bimetallic nickel-cobalt nanoclusters with gallium nitride nanowires on silicon wafer for light-driven hydrogen production from methanol. Under concentrated light illumination, an excellent hydrogen evolution rate and stability is achieved without additional energy input. Outdoor tests validated the viability of the architecture for hydrogen evolution from methanol under natural concentrated sunlight conditions.

Author Manuscript

This article is protected by copyright. All rights reserved.

Author Manuscript



This article is protected by copyright. All rights reserved.